Applied Physics Letters

Material and device properties of superacid-treated monolayer molybdenum disulfide

Cite as: Appl. Phys. Lett. **110**, 033503 (2017); https://doi.org/10.1063/1.4974046
Submitted: 06 November 2016 . Accepted: 30 December 2016 . Published Online: 18 January 2017

Abdullah Alharbi, Percy Zahl, and Davood Shahrjerdi

Material and device properties of superacid-treated monolayer molybdenum disulfide

Abdullah Alharbi,[1] Percy Zahl,[2] and Davood Shahrjerdi[1,a)]
[1]*Electrical and Computer Engineering, New York University, Brooklyn, New York 11201, USA*
[2]*Center for Functional Nanomaterials, Brookhaven National Laboratory, Upton, New York 11973, USA*

(Received 6 November 2016; accepted 30 December 2016; published online 18 January 2017)

We study the effects of chemical treatment with bis(trifluoromethane) sulfonimide superacid on material and device properties of monolayer molybdenum disulfide grown by chemical vapor deposition. Our spatially resolved photoluminescence (PL) measurements and device studies reveal two key findings due to the chemical treatment: (1) noticeable transformation of trions to neutral excitons, and (2) over 7-fold reduction in the density of mid-gap trap states. Specifically, a combination of scanning Auger microscopy and PL mapping reveals that the superacid treatment is effective in passivating the sulfur-deficient regions. *Published by AIP Publishing.*
[http://dx.doi.org/10.1063/1.4974046]

Two-dimensional (2-D) transition metal dichalcogenides (TMDs) have potential for making a wide range of optoelectronic and electronic devices such as photovoltaics,[1] photodetectors,[2–4] and field–effect transistors (FETs).[5–7] In all cases, the device performance strongly depends on the inherent material properties such as carrier mobility and minority carrier lifetime. However, structural disorders degrade these key material properties and the ensuing device performance. It is, therefore, essential to reduce the structural disorders during the synthesis or the post-synthesis steps using chemical treatments. The microelectronic industry has continually applied these strategies for reducing defects in semiconductor materials and their interfaces with dielectrics. Examples include passivation of interfacial defects by incorporating chlorine,[8] hydrogen,[9] or sulfur atoms.[10,11]

Many studies demonstrated the presence of high structural defects in 2-D TMD films prepared through mechanical exfoliation or chemical vapor deposition (CVD). Those structural disorders include various types of point defects, grain boundaries, and complex dislocations.[12–14] Research is ongoing to develop effective chemical treatment methods for mitigating the detrimental impact of the structural defects on key material properties. Among those, Amani *et al*. has shown remarkable improvement in the quantum yield and the photoluminescence intensity for exfoliated and CVD sulfur-based TMDs via the chemical treatment using bis(trifluoromethane) sulfonimide (TFSI) superacid.[15–17] They attributed the observed improvements to the reduction of sulfur-based defects, where a TFSI-mediated hydrogenation process causes the rearrangement of sulfur adatoms on the surface. However, more work needs to be done to quantify the effect of the superacid treatment on the density of defects in molybdenum disulfide (MoS_2) films. In addition, from the work of Amani *et al*., the surface passivation using superacid appears to be thermally stable, at least up to 300 °C. This opens up the opportunity to investigate the effect of the superacid treatment on the interface properties between MoS_2 and high-k dielectrics in a top-gated device configuration. Such device studies are currently missing in the literature.

In this work, we investigate the material and device properties of MoS_2 upon treatment by TFSI superacid (Sigma-Aldrich). We observed noticeable transformation of trions to neutral excitons due to the superacid treatment. Scanning Auger microscopy (SAM) measurements reveal that the transformation of trions to excitons is more pronounced in regions with lower sulfur to molybdenum ration (S/M). Further, we fabricated top-gated FETs on as-grown and TFSI-treated CVD MoS_2 films. Our electrical measurements indicate that the TFSI treatment improves the subthreshold swing and reduces the density of mid-gap traps.

We initially used exfoliated flakes to optimize the chemical treatment process. We produced monolayer flakes through mechanical exfoliation of MoS_2 bulk crystals (SPI Supplies). The monolayer flakes underwent TFSI treatments in a glovebox system with low oxygen and moisture levels below 10 ppm. This is to prevent the possible oxidation of the MoS_2 films during the TFSI treatment. The enhancement of the PL intensity guided our experiments for finding the optimal treatment conditions. We found relatively weak dependence of the PL improvement on the concentration of the TFSI solution. In our experiments, we first dissolve 20 mg of TFSI in 1 ml of 1,2-dichloroethane (DCE) (Sigma-Aldrich), and further dilute it to ~2 mM. The samples were placed in a tightly sealed glass vial with 3 mL of TFSI solution, followed by heating the vials on a hot plate at 120 °C for 10–20 min. The samples were then dried using nitrogen and baked on a hot plate at 100 °C for 5 min. Using this process, we observed over 40-fold increase in the PL intensity of the exfoliated MoS_2 flakes, measured at 20 μW laser excitation power (Fig. 1(a)).

The PL spectrum of MoS_2 at monolayer thickness consists of charged trions and neutral excitons with overlapping emission energies[18] (see supplementary material). Curve fitting using the Gaussian function is typically used for analyzing the PL spectra. It is, however, difficult to use this approach for analyzing a large amount of spatially resolved PL data. Bao *et al*. has shown the effectiveness of the

a)Email: davood@nyu.edu

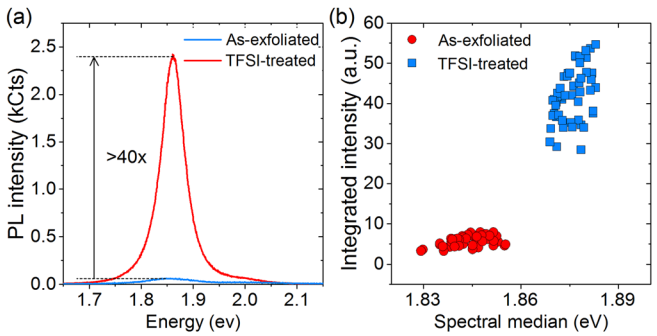

FIG. 1. (a) Enhancement of the PL intensity guided the optimization of the chemical treatment process. (b) The spectral median analysis reveals the transformation of trions to excitons upon TFSI treatment.

spectral median method for qualitative analysis of the spatial PL maps.[19] The spectral median method is particularly useful to illustrate the relative population of the charged trions to the neutral excitons and to show the shift in the emission energy of those excitons. We have adopted this method for analyzing the spatial PL maps of the MoS_2 flakes before and after the treatment with TFSI. In this method, the spectral median is defined at the energy that splits the PL spectrum into two regions with equal integrated intensities[19] (see supplementary material).

Previous reports demonstrated the shift in the excitonic energies of the monolayer MoS_2 upon increasing the laser excitation power.[20–22] We made similar observation by studying the power-dependence of the PL spectrum (see supplementary material). This observation signals the increase in the relative emission of trions to neutral excitons possibly due to the significant increase in the non-radiative exciton-exciton interactions at a high excitation laser power density.[17] In our chemical treatment studies, we used a laser excitation power of $\sim 200\,\mu W$ with an estimated laser spot of $\sim 2\,\mu m$ to create a discernable trion emission and subsequently examine their possible transformation mediated by the TFSI treatment. Many factors influence the population of charged trion states, including chemical doping[23] and electrostatic doping.[24] Further, the presence of sulfur vacancies in the lattice facilitates trion emission because of the enhanced local charge transfer at these defect sites.[25] Our aim is to investigate the possible reduction of the charged and defect-bound trions in exfoliated and CVD MoS_2 flakes upon TFSI treatment. The scatter plot in Fig. 1(b) shows the integrated intensity as a function of the spectral median for each position in the PL spatial maps of an exfoliated flake measured before and after the chemical treatment (Fig. S2 in supplementary material). This plot illustrates the shift in the spectral emission of MoS_2 to higher energies upon TFSI treatment, thus qualitatively indicating the effectiveness of this chemical treatment for reducing the density of trions. Furthermore, we used the approach by Su *et al.*[26–28] for analyzing the effect of the superacid treatment on various excitonic states in the PL spectra of the exfoliated flake (Fig. S3 in supplementary material). Our analysis shows the reduction of defect-bound excitons and also the reduction of charged trions upon treatment with TFSI superacid.

We now proceed to study the effect of the TFSI treatment on CVD MoS_2. Large-area synthesis of high-quality TMDs is a necessary step for enabling a commercially viable technology based on these materials. Synthesis through CVD is a popular approach for growing monolayer MoS_2 on SiO_2/Si substrates.[12,29] We produced monolayer MoS_2 flakes on p^+ silicon with the 285 nm SiO_2 capping layer through CVD using molybdenum trioxide (6 mg) and sulfur ($\sim$100 mg) solid precursors at 850 °C. The details of the growth process are described in the supplementary material. Interestingly, our as-grown monolayer CVD MoS_2 flakes exhibit about 10-fold stronger PL emission than the as-exfoliated flakes at a given excitation power. To understand the effect of TFSI superacid on the CVD flakes, the samples underwent a treatment process similar to the exfoliated flakes, described earlier. We found this recipe to give the highest PL enhancement for the CVD samples as well.

Fig. 2(a) shows the spatially resolved spectral median and integrated intensity for a CVD flake. This flake comprises two merged triangles. Similar to the previous reports on monolayer CVD MoS_2, [30] we found out that the flakes are under biaxial tension (Fig. S4 in supplementary material). The spatial spectral median map of the as-grown MoS_2 in Fig. 2(a) clearly shows the shift of the spectral median to higher emission energies near the grain boundary (GB) between the two flakes. The shift to higher emission energies near the intraflake GB is possibly due to defect-induced relaxation. Upon the chemical treatment, we observe the non-uniform change of the spectral median and the integrated intensity of the PL across the film upon TFSI treatment, shown in Fig. 2(b). We also performed elemental characterization of the CVD flake using scanning Auger microscopy to examine the stoichiometry of the CVD film. Fig. 2(c) shows the scanning electron microscopic image of the CVD film. The gold ring was deposited to reduce the charging effect during the measurements. Fig. 2(d) shows the Auger spectra measured at four different locations on the flake, marked A, B, C, and D. The locations corresponding to these points are also marked on the PL maps in Fig. 2(a). The summary of the sulfur to molybdenum peak ratio from the Auger measurements together with the corresponding change in the PL spectral median (ΔE) is shown in Table I. Our results suggest that the TFSI treatment is effective in passivating defects in the sulfur-deficient regions. Note that the tensile strain in the film is unchanged upon the superacid treatment, confirmed by Raman spectroscopy (Fig. S5 in supplementary material).

Next, we examine the effect of the chemical treatment on the electronic properties of top-gated FETs, fabricated on monolayer CVD MoS_2 films. The schematic illustration of the device is shown in Fig. 3(a). After the CVD growth, the sample was split into two pieces. The candidate flakes for making devices had similar initial PL intensities. The two pieces were processed together. The samples initially underwent electron-beam lithography (EBL), reactive ion etching in CF_4/O_2 plasma, and electron beam evaporation of silver/gold (Ag/Au, 15 nm/30 nm) to define the device active regions and to form the source/drain metal electrodes. Next, one of the samples (sample 1) underwent the TFSI treatment, while the other sample (sample 2) skipped this step. We noticed that Ag contacts withstand the TFSI treatment. We then formed 20 nm of hafnium oxide (HfO_2) gate dielectric

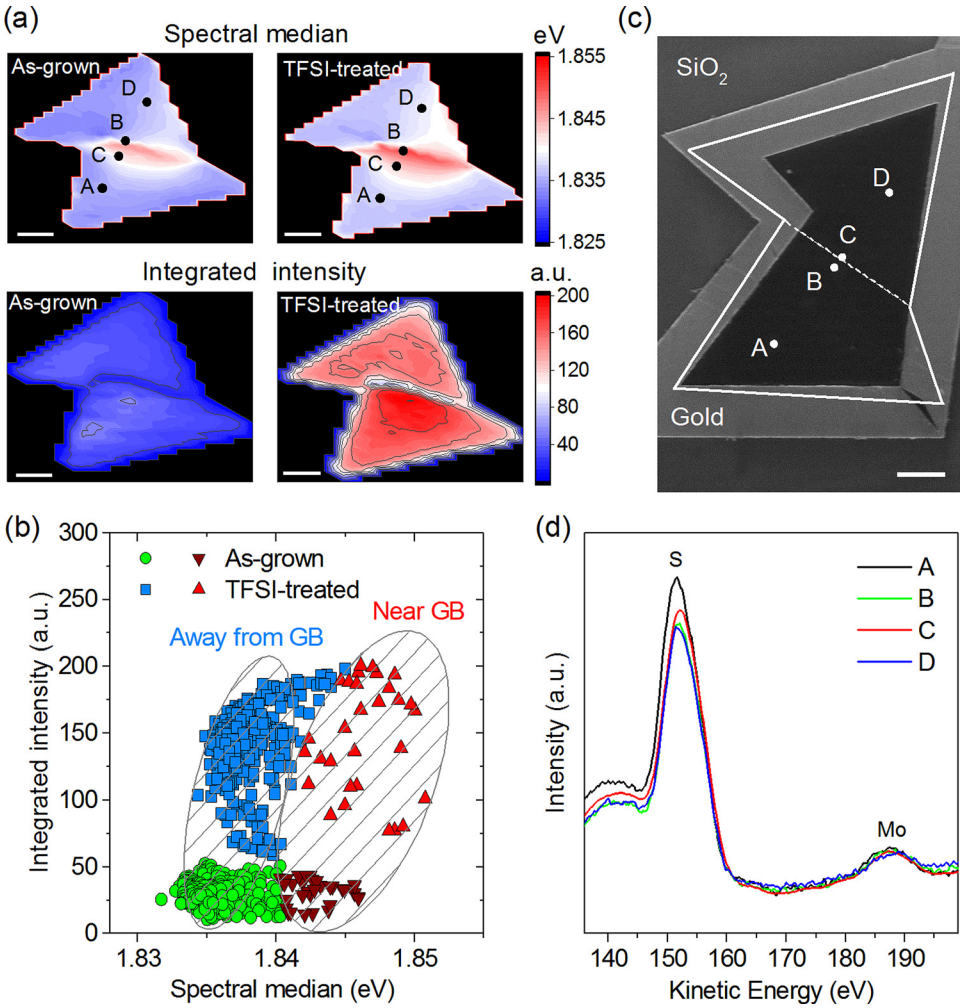

FIG. 2. (a) The spatial analysis of the PL spectra using the spectral median method for a monolayer CVD MoS_2 flake before and after the TFSI treatment process. (b) Shift in the excitonic energies due to the TFSI treatment is more pronounced near the intra-flake grain boundary, possibly due to the presence of high sulfur vacancy. (c) The SEM image of the CVD flake. The solid line shows the edge of the flake, and the dashed line represents the approximate location of the GB. (d) Auger spectra corresponding to four different locations on the flake, marked A, B, C, and D. The scale bars are 4 μm.

on these samples using atomic layer deposition (ALD) at 200 °C. A previous report indicates the thermal stability of the TFSI treatment at temperatures as high as 300 °C.[16] Finally, the metal gate electrode was made through EBL patterning and lift-off of chrome/gold (Cr/Au, 10 nm/40 nm).

Fig. 3(b) shows the representative transfer characteristics of two devices on samples 1 and 2. We noticed that the TFSI-treated samples generally exhibit slightly better subthreshold swing than their as-grown counterparts. The TFSI and non-TFSI treated devices exhibit nearly similar drive currents, suggesting that those devices have comparable carrier mobility and contact resistance. Using the approach in Ref. 31, we estimated the carrier mobility and the contact resistance of both devices to be ~12 cm^2/V s and ~1 kΩ.

We performed capacitance-voltage measurements to quantify the density of the localized gap states in these devices. The large size of the CVD flakes allows the fabrication of adequately large devices for making capacitance-voltage measurements. Figs. 4(b) and 4(c) show the corresponding capacitance-frequency characteristics of the devices on samples 1 and 2, respectively. Interestingly, the TFSI-treated device exhibits noticeably smaller frequency dispersion than the as-grown device, suggesting the effectiveness of the TFSI process in reducing the density of trap states. We used the equivalent device model shown in Fig. 4(a) to determine the density of localized gap states.[32,33] In this model, C_{it} is the interface trap capacitance and is given by qD_{it}, where q is the elementary charge and D_{it} is the density of

TABLE I. Summary of Auger and PL measurements of the CVD flake in Fig. 2. The shift of the PL spectral median due to the chemical treatment is higher in the regions with lower S/Mo ratio.

Point	S_{Peak}/Mo_{Peak}	ΔE (meV)
A	11.7 ± 0.2	2 ± 0.3
B	10.7 ± 0.19	4.6 ± 0.5
C	10.96 ± 0.2	5.5 ± 0.8
D	10.8 ± 0.21	4.2 ± 0.6

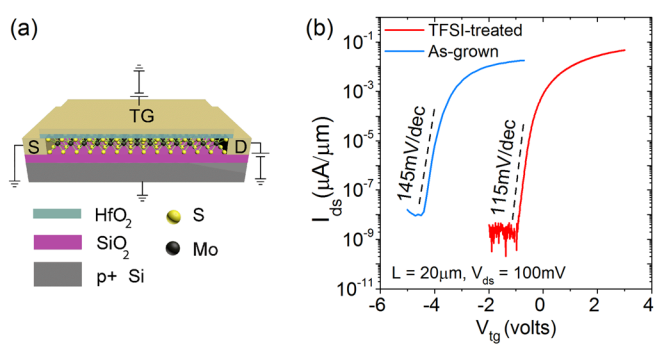

FIG. 3. (a) Schematic of the top-gated MoS_2 FET. (b) Effect of the TFSI treatment on the transfer characteristics of CVD MoS_2 FETs.

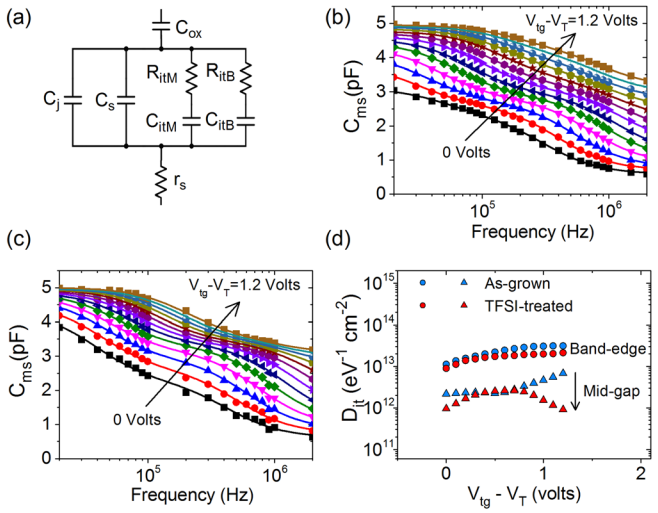

FIG. 4. (a) The electrical device model used for extracting the density of mid-gap and band-edge trap states from the measured series model. Corresponding capacitance-frequency characteristics of the (b) as-grown and (c) TFSI-treated devices in Fig. 3(b) as a function of the gate voltage overdrive. (d) The extracted mid-gap and bandage trap density.

traps. The resistance in series with C_{it} (R_{it}) represents the trap resistance and is given by τ_{it}/C_{it}, where τ_{it} is the time constant of the traps. We used two types of traps for fitting the capacitance data, namely, the mid-gap and the band-edge traps denoted by "M" and "B" subscripts in that model. The solid curves in Figs. 4(b) and 4(c) represent the fitted curves. Fig. 4(d) illustrates the corresponding density of mid-gap and band-edge trap states for the devices in Fig. 3(b). The fitting results show the reduction of the trap density for the TFSI-treated device. Theoretical studies suggest that sulfur vacancies in monolayer MoS_2 manifest themselves through deep trap states in the energy gap.[34] Therefore, we surmise that the smaller density of the mid-gap states in the TFSI-treated device is attributed to the passivation of sulfur-based defects by TFSI, which is consistent with our PL studies.

In summary, we have demonstrated the effectiveness of the chemical treatment using the TFSI superacid in passivating defects in sulfur-deficient regions. We analyzed the spatial PL data for both exfoliated and CVD monolayer MoS_2 flakes using the spectral median method. The PL studies demonstrated the increase in the relative emission of neutral excitons to the charged trions upon TFSI treatment. The comparison of the electrical characteristics of the as-grown and the TFSI-treated top-gated FETs fabricated on CVD flakes indicates the effectiveness of TFSI treatment in reducing the density of the mid-gap traps.

See supplementary material for additional details on the CVD MoS_2 synthesis, material and device characterization.

The authors acknowledge Borui Liu for the initial help with some of the TFSI treatments. This work was supported in part by NSF award #1638598. This research used resources of the Center for Functional Nanomaterials, which is a U.S. DOE Office of Science Facility, at Brookhaven National Laboratory under Contract No. DESC0012704.

A.A. and D.S. designed and carried out the experiments. P.Z. contributed to Auger measurements.

[1]A. Dashora, U. Ahuja, and K. Venugopalan, Comput. Mater. Sci. **69**, 216 (2013).
[2]H. S. Lee, S.-W. Min, Y.-G. Chang, M. K. Park, T. Nam, H. Kim, J. H. Kim, S. Ryu, and S. Im, Nano Lett. **12**, 3695 (2012).
[3]O. Lopez-Sanchez, D. Lembke, M. Kayci, A. Radenovic, and A. Kis, Nat. Nano **8**, 497 (2013).
[4]Z. Yin, H. Li, H. Li, L. Jiang, Y. Shi, Y. Sun, G. Lu, Q. Zhang, X. Chen, and H. Zhang, ACS Nano **6**, 74 (2012).
[5]S. Ghatak, A. N. Pal, and A. Ghosh, ACS Nano **5**, 7707 (2011).
[6]B. Radisavljevic, A. Radenovic, J. Brivio, I. V. Giacometti, and A. Kis, Nat. Nanotechnol. **6**, 147 (2011).
[7]A. Ayari, E. Cobas, O. Ogundadegbe, and M. S. Fuhrer, J. Appl. Phys. **101**, 14507 (2007).
[8]R. Kriegler, Y. Cheng, and D. R. Colton, J. Electrochem. Soc. **119**, 388 (1972).
[9]M. L. Reed and J. D. Plummer, J. Appl. Phys. **63**, 5776 (1988).
[10]D. Shahrjerdi, E. Tutuc, and S. K. Banerjee, Appl. Phys. Lett. **91**, 063501 (2007).
[11]M. M. Frank, S. J. Koester, M. Copel, J. A. Ott, V. K. Paruchuri, H. Shang, and R. Loesing, Appl. Phys. Lett. **89**, 112905 (2006).
[12]A. M. van der Zande, P. Y. Huang, D. A. Chenet, T. C. Berkelbach, Y. You, G.-H. Lee, T. F. Heinz, D. R. Reichman, D. A. Muller, and J. C. Hone, Nat. Mater. **12**, 554 (2013).
[13]W. Zhou, X. Zou, S. Najmaei, Z. Liu, Y. Shi, J. Kong, J. Lou, P. M. Ajayan, B. I. Yakobson, and J.-C. Idrobo, Nano Lett. **13**, 2615 (2013).
[14]D. Liu, Y. Guo, L. Fang, and J. Robertson, Appl. Phys. Lett. **103**, 183113 (2013).
[15]M. Amani, R. A. Burke, X. Ji, P. Zhao, D.-H. Lien, P. Taheri, G. H. Ahn, D. Kiriya, J. W. Ager, and E. Yablonovitch, ACS Nano **10**, 6535 (2016).
[16]M. Amani, D.-H. Lien, D. Kiriya, J. Xiao, A. Azcatl, J. Noh, S. R. Madhvapathy, R. Addou, K. Santosh, and M. Dubey, Science **350**, 1065 (2015).
[17]M. Amani, P. Taheri, R. Addou, G. H. Ahn, D. Kiriya, D.-H. Lien, J. W. Ager III, R. M. Wallace, and A. Javey, Nano Lett. **16**, 2786 (2016).
[18]K. F. Mak, K. He, C. Lee, G. H. Lee, J. Hone, T. F. Heinz, and J. Shan, Nat. Mater. **12**, 207 (2013).
[19]W. Bao, N. J. Borys, C. Ko, J. Suh, W. Fan, A. Thron, Y. Zhang, A. Buyanin, J. Zhang, S. Cabrini, P. D. Ashby, A. Weber-Bargioni, S. Tongay, S. Aloni, D. F. Ogletree, J. Wu, M. B. Salmeron, and P. J. Schuck, Nat. Commun. **6**, 7993 (2015).
[20]H. Taghinejad, M. Taghinejad, A. Tarasov, M.-Y. Tsai, A. H. Hosseinnia, P. M. Campbell, A. A. Eftekhar, E. M. Vogel, and A. Adibi, preprint arXiv:1502.00593 (2015).
[21]Y. Kim, Y. Jhon, J. Park, C. Kim, S. Lee, and Y. Jhon, Sci. Rep. **6**, 21405 (2016).
[22]S. Tongay, J. Suh, C. Ataca, W. Fan, A. Luce, J. S. Kang, J. Liu, C. Ko, R. Raghunathanan, and J. Zhou, Sci. Rep. **3**, 2657 (2013).
[23]S. Mouri, Y. Miyauchi, and K. Matsuda, Nano Lett. **13**, 5944 (2013).
[24]M. Buscema, G. A. Steele, H. S. van der Zant, and A. Castellanos-Gomez, Nano Res. **7**, 561 (2014).
[25]H. Nan, Z. Wang, W. Wang, Z. Liang, Y. Lu, Q. Chen, D. He, P. Tan, F. Miao, and X. Wang, ACS Nano **8**, 5738 (2014).
[26]W. Su, H. Dou, D. Huo, N. Dai, and L. Yang, Chem. Phys. Lett. **635**, 40 (2015).
[27]W. Su, L. Jin, X. Qu, D. Huo, and L. Yang, Phys. Chem. Chem. Phys. **18**, 14001 (2016).
[28]W. Su, N. Kumar, S. J. Spencer, N. Dai, and D. Roy, Nano Res. **8**, 3878 (2015).
[29]S. Najmaei, Z. Liu, W. Zhou, X. Zou, G. Shi, S. Lei, B. I. Yakobson, J.-C. Idrobo, P. M. Ajayan, and J. Lou, Nat. Mater. **12**, 754 (2013).
[30]Z. Liu, M. Amani, S. Najmaei, Q. Xu, X. Zou, W. Zhou, T. Yu, C. Qiu, A. G. Birdwell, F. J. Crowne, R. Vajtai, B. I. Yakobson, Z. Xia, M. Dubey, P. M. Ajayan, and J. Lou, Nat. Commun. **5**, 5246 (2014).
[31]T. Roy, M. Tosun, J. S. Kang, A. B. Sachid, S. B. Desai, M. Hettick, C. C. Hu, and A. Javey, ACS Nano **8**, 6259 (2014).
[32]W. Zhu, T. Low, Y.-H. Lee, H. Wang, D. B. Farmer, J. Kong, F. Xia, and P. Avouris, Nat. Commun. **5**, 3087 (2014).
[33]A. Alharbi and D. Shahrjerdi, Appl. Phys. Lett. **109**, 193502 (2016).
[34]M. Pandey, F. A. Rasmussen, K. Kuhar, T. Olsen, K. W. Jacobsen, and K. S. Thygesen, Nano Lett. **16**, 2234 (2016).